Original Article
J. Korean Wood Sci. Technol. 2026, 54(3): 308-324
https://doi.org/10.5658/WOOD.2026.54.3.308

Journal of the Korean Wood Science and Technology
pISSN: 1017-0715 eISSN: 2233-7180
http://www.woodj.org

Performance of the Potanje Beam–Column Connection System in the Souraja Traditional House of Central Sulawesi

Muhammad Yusuf AMIR[1,2] · Ali AWALUDIN[1,†] · Iman SATYARNO[1] · Muh Fauzie SISWANTO[1]

ABSTRACT

A *Potanje* joint is a full-penetration *mortise–tenon* connection equipped with a wedge, providing friction-based energy dissipation similar to that of the Japanese P-type joint, which uses a single wedge without dowels. In the *Potanje* configuration, the dowels primarily restrain beam sliding and improve deformation control under cyclic loading. This study aimed to evaluate the seismic performance of the *Potanje* beam–column connection system used in traditional *Souraja* houses in Palu City, Indonesia. To further enhance cyclic performance, two modified configurations (D-type and T-type) were proposed by incorporating double wedges combined with additional dowels; their performance was evaluated against the original *Potanje*-type and Japanese P-type connections. A total of 11 beam–column joint specimens of ironwood species were tested under cyclic displacement-controlled loading following ASTM procedures, and the experimental data were validated using three-dimensional finite element models. The results demonstrated that although *Potanje*-type and P-type connections achieved higher moment capacities, the modified connections exhibited greater ductility and more stable equivalent viscous damping ratios over repeated cycles. Both experiments and numerical simulations showed wedge-controlled damage initiation, demonstrating its potential as a primary energy-dissipation component. The modified D- and T-type connections exhibited superior seismic resistance, demonstrating potential for application in earthquake-resistant timber structures that do not utilize modern mechanical fasteners.

Keywords: *Potanje* beam–column connections, cyclic loading, dowel, finite element analysis, wedge

1. INTRODUCTION

The *Souraja* traditional house [Fig. 1(a)] is a historical building type found in Palu City, Indonesia, constructed from ironwood (*Eusideroxylon zwageri*). This stilt house (pile dwelling) uses a column system and is unique in its beam–column connections, which is a full-penetration knock-down/*mortise–tenon* system with wedges and dowels, as illustrated in Fig. 1(b). The *Souraja* house has remained standing since 1892, surviving several major earthquakes that caused the collapse of surrounding buildings; these include events in 1907, 1909, 1937, 2012, and the September 2018 earthquake, which had a magnitude of 7.4 M (PuSGeN, 2018).

The beam–column joint in the *Souraja* house is *mortise–tenon* connection system utilizing a wedge, locally referred to as *Potanje* (where the beam is termed *polaya* and the column *tinja*). A previous study by

Date Received September 30, 2025; Date Revised December 3, 2025; Date Accepted February 25, 2026; Published May 25, 2026
[1] Civil Engineering and Environment Department, Gadjah Mada University, Yogyakarta 55284, Indonesia
[2] Civil Engineering Department, University of Muhammadiyah Palu, Palu 94118, Indonesia
[†] Corresponding author: Ali AWALUDIN (e-mail: ali.awaludin@ugm.ac.id, https://orcid.org/0000-0003-2330-1685)

(a) (b)

Fig. 1. *Souraja* traditional house. (a) Front view of a *Souraja* house, (b) *Potanje* beam–column connection system with wedge and dowel.

Tanahashi *et al.* (2014) identified four distinct wedge types, as (Fig. 2): the T-type, comprising several triangular pieces with a slope of approximately 1/10 to 1/6; the C-type, consisting of two triangular pieces with slightly curved slopes; the P-type, featuring a wedge with a slight slope at the corners to facilitate insertion into the column; and the D-type, representing a pair of triangular chips inserted separately from opposite sides that behave independently. Tanahashi *et al.* (2014) proposed that the best wedges are C-, T-, and D-types. In comparison, the C- and T-types exhibited superior moment-retaining abilities but often experienced a decrease in stiffness compared to the D-type. This suggests that the beam–column connection with the wedge system can effectively reduce earthquake forces, where the friction generated produces a frictional damper.

The beam–column connection of the *Potanje* system, also known as *mortise–tenon*, is structurally similar to that of the P-type wedge, but is reinforced with a dowel, as illustrated in Fig. 3. Several *mortise–tenon* designs,

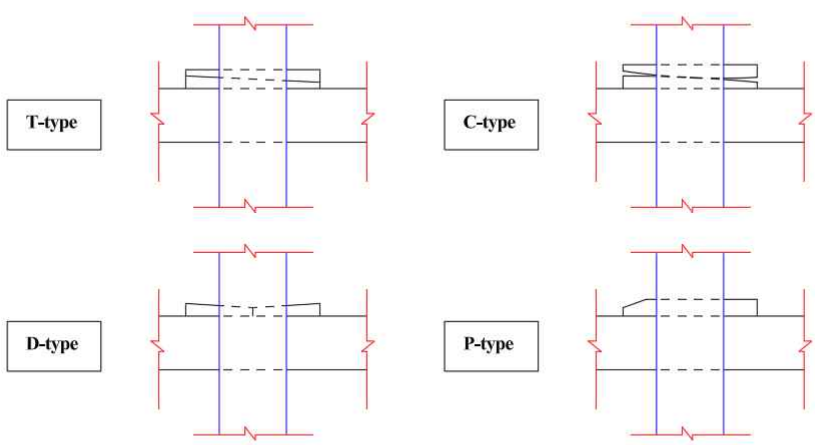

Fig. 2. Wedge types used in the testing. Adapted from Tanahashi *et al*. (2014) with permission of the copyright holder.

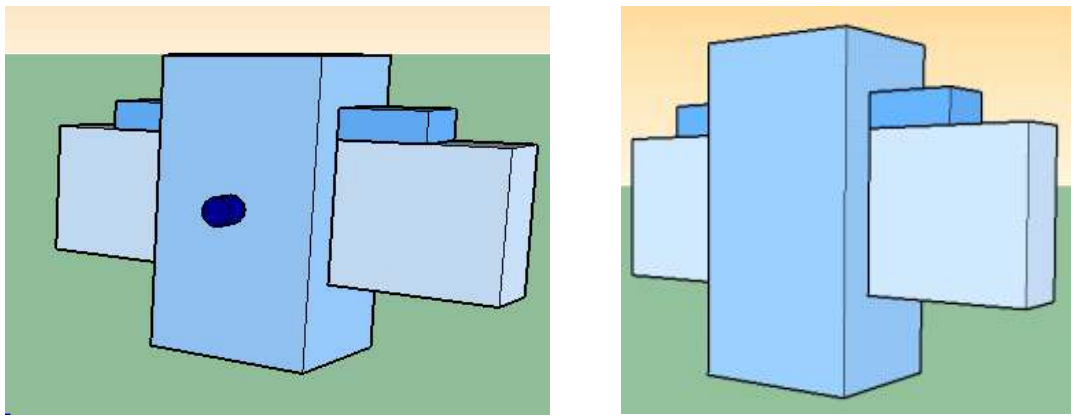

(a) (b)

Fig. 3. Beam–column connection with wedges. (a) *Potanje*-type, (b) P-type.

such as full- and half-penetration, incorporate wedges and dowels to prevent beam displacement and ensure rigidity. Maeno *et al.* (2004) conducted static lateral and shaking table tests on traditional wooden buildings with a *mortise–tenon* system and wedge. Their results demonstrated that under small structural deformations, the restoring force was governed by column rocking. However, as deformation increased, the bending moments from the tie beam became more dominant than those generated by the restoring force. Similar *mortise–tenon* testing, which compares full and half penetration with a locking beam, was conducted by Yeo *et al.* (2016). Dong *et al.* (2023) tested both types of *mortise–tenon* with light steel reinforcement and observed that the half-penetration type exhibited larger moment resistance capabilities than the full-penetration type. Furthermore, Yu *et al.* (2022) explored *mortise–tenon* connections strengthened with innovative metal dampers and reported that the full-penetration type (straight and penetrated *tenon*) exhibited superior performance than the half-penetration type (dovetail *tenon*). Suesada *et al.* (2019) conducted a full-penetration *mortise–tenon* test with hardwood reinforcement, while Wu *et al.* (2019) investigated full-penetration *mortise–tenon* connection with slot-in bamboo scriber plates reinforcement. Their findings demonstrated enhanced resistance performance, specifically in terms of rotational stiffness and moments compared to that of unreinforced beams.

Tanahashi *et al.* (2014) explored a full-penetration *mortise–tenon* with various wedge types, leading to good seismic damping of the beam–column system with D-, C-, and T-type wedges. Fujita *et al.* (2016) investigated full-penetration *mortise–tenon*s with wedges using a transition beam; they demonstrated an initial stiffness 50% lower than that of a beam without joints and bending failure at deformation angles from 1/10 to 1/7 rad. Hassan *et al.* (2010) examined half-penetration and observed that *mortise–tenon* joints with steel dowels exhibited better moment and shear resistance than those of wooden joints.

Based on the aforementioned description, this study aims to evaluate the performance of the *Potanje*-type joint and the D- and T-type modified systems– both of which are full-penetration *mortise–tenon* joints utilizing wedges and dowels–and compare their behavior to that of the P-type system (Fig. 3). The performance of these connections was evaluated based on strength, ductility, and damping ratio; subsequently, the experimental results were validated via numerical analysis. In these systems, the wedge contributes to the mitigation of seismic

forces, while the dowels serve to prevent beam displacement. The damping performance was quantified using the damping ratio, which represents the capacity of a structure to dissipate input energy through changes in shape, fatigue, and progressive damage. A higher damping ratio indicates a superior ability of the structure to absorb energy. The novelty of this study lies in the evaluation of wedge-based connections reinforced with dowels in beam–column joints, a configuration that has not been reported in previous investigations.

2. MATERIALS and METHODS

2.1. Materials

Ironwood (*E. zwageri*) used in the *Souraja* building structures was selected due to its widespread application in traditional architecture and superior mechanical performance. The material exhibited a modulus of elasticity of 13,704 MPa, a modulus of rupture of 115.46 MPa, a density of 1,040 kg/m^3, and a moisture content 19.73%. Preliminary tests determined the physical properties according to ASTM D4442-92 (ASTM, 2003b; Hadi *et al*., 2022; Kim *et al*., 2024; Lee *et al*., 2024; Seta *et al*., 2023) and the mechanical properties according to ASTM D143-94 (ASTM, 1994; Cha *et al*., 2022; Mawardi *et al*., 2025; Nugroho *et al*., 2024; Rofii *et al*., 2024; Song and Kim, 2023).

To ensure consistency with existing structures, the geometric configuration of the *Souraja* building was defined based on field measurements. The column spacing was 3,500 mm, with a ground-floor height of 2,540 mm, and a first-floor height of 2,920 mm (Fig. 4). The detailed structural dimensions are summarized in Table 1.

Cyclic loading tests were conducted on wedge-based beam–column joint specimens consisting of four configurations: *Potanje*-type (two specimens), P-type (three specimens), modified D-type (three specimens), and modified T-type (three specimens; Fig. 5). While the *Potanje*-type connection is similar to the P-type, the

Table 1. Structural geometry of the *Souraja* building

Wood type	Ironwood (mm)
Column	160 × 160
Main beam	70 × 140
Floor beam	70 × 90
Floor board	20 × 200
Roof truss	70 × 90

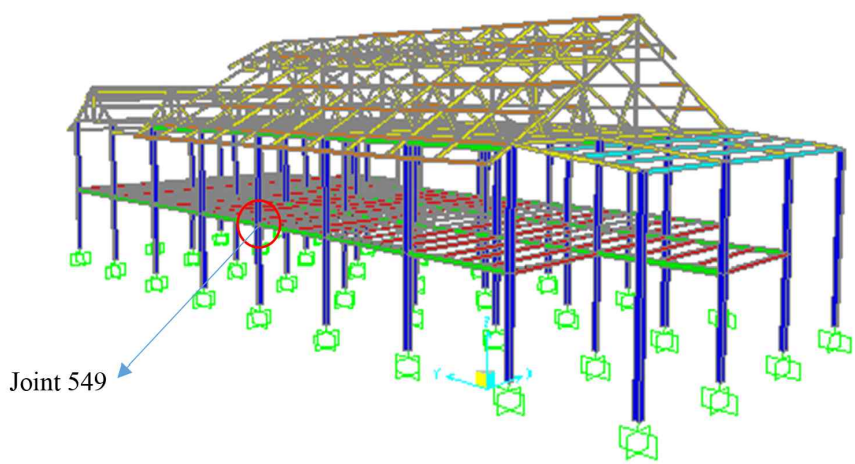

Fig. 4. *Souraja* traditional building structure in SAP2000.

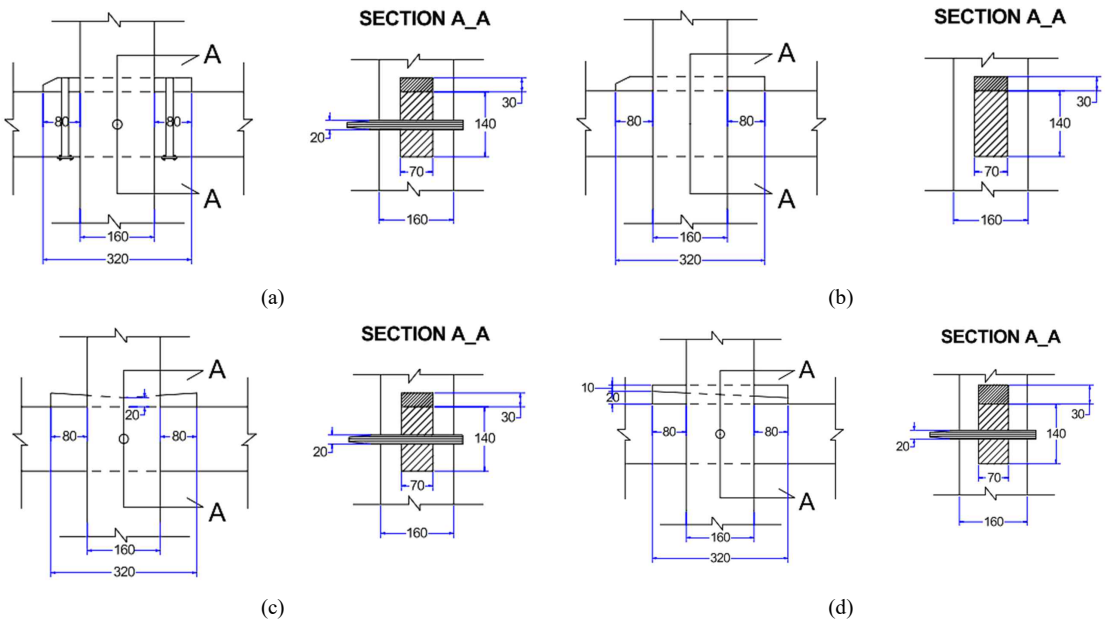

Fig. 5. Connection types and dimensions (mm) used for experimental testing. (a) *Potanje*-type (Pj), (b) P-type (P), (c) modified D-type (D), (d) modified T-type (T).

former is reinforced with dowels, whereas the latter is not. For the *Potanje*-type, clamps were installed on the wedge and beam to replicate *in situ* structural conditions. Correspondingly, the modified D- and T-type joints represent the original D- and T-type joints strengthened with dowels.

2.2. Methods

Prior to laboratory testing, the *Souraja* building was modeled using SAP 2000 to determine boundary conditions and internal bending moments acting on the experimental specimens, specifically at joint 549. The column was modeled as a fixed support (Fig. 4). Geometric parameters were used as input variables for numerical analysis; structural responses are listed in Table 2.

Cyclic loading was applied laterally to the frame following a monotonic displacement protocol based on the drift ratios in accordance with ASTM E2126-02a (ASTM, 2003a; Lee and Jang, 2023; Fig. 6). Subsequently, displacements were measured using five linear

Table 2. Output of beam–column at joint 549

Item	Length (m)	Moment A (kNm)	Moment B (kNm)	Point M = 0 (m)
Top column	2.92	3.73	4.76	1.23
Bottom column	2.54	2.42	6.54	0.67
Left beam	3.50	3.08	3.07	1.75
Right beam	3.50	3.08	3.08	1.75

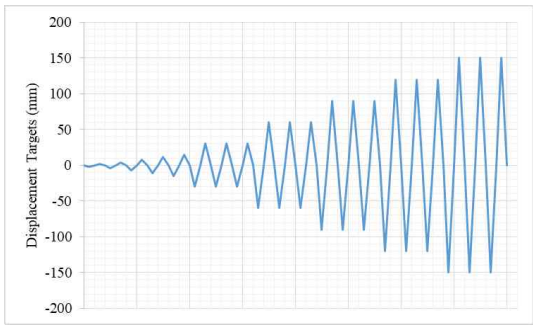

Fig. 6. Loading protocol.

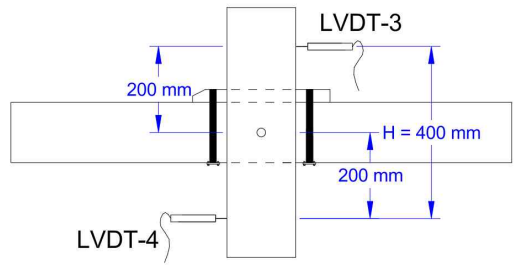

Fig. 8. LVDT position on wood joints (LVDT-3: top column and LVDT-4: bottom column). LVDT: linear variable differential transducer.

variable differential transducers (LVDTs): LVDT-1 controlled the actuator displacement, LVDT-2 recorded the load displacement relationship, LVDT-3 and LVDT-4 captured joint rotations, and LVDT-5 controlled beam displacement (Fig. 7). Each LVDT had a maximum stroke of 300 mm, thereby limiting the target displacement of LVDT-2 to 150 mm.

The rotation angle θ (Li *et al.*, 2021) was calculated based on two displacement transducers (LVDT-3 and LVDT-4) and the column side (Fig. 8). Neglecting bending deformation in the beam, the joint rotation angle was calculated from the displacement values of two transducers:

$$\theta = \frac{\triangle_2 - \triangle_1}{H} \quad (1)$$

where: θ = rotation angle (rad); $\triangle_1$ = displacement measured by LVDT-4 (mm); $\triangle_2$ = displacement measured by LVDT-3 (mm); H = distance of LVDT-3 and LVDT-4 (mm).

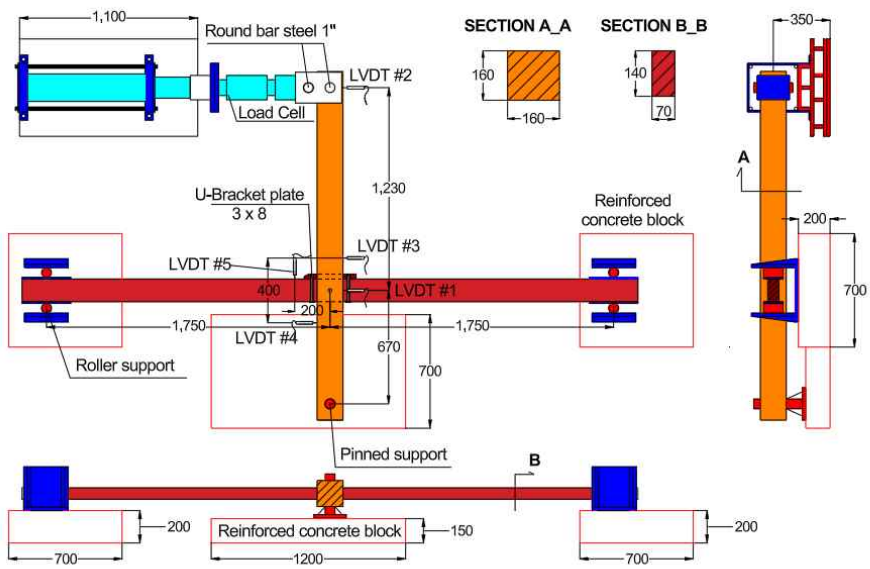

Fig. 7. Experimental setup (dimensions are expressed in mm).

Rotational ductility is determined by ultimate rotation (θ_u) and yield rotation (θ_y). The ultimate moment (M_u) and yield moment (M_y) were determined according to ASTM E2126-02a (ASTM, 2003a), with the yield point defined as $0.5M_u$ according to the Karacabeyli and Ceccotti method (Muñoz, 2008). The rotational ductility (Maras *et al.*, 2024) was determined as follows:

$$D = \frac{\theta_u}{\theta_y} \quad (2)$$

where: D = ductility; θ_u = ultimate rotation; θ_y = yield rotation.

The ductility coefficient (D) describes joint ductility and is often defined as the ratio of the ultimate rotation to the yield rotation. Specifically, the ductility scale proposed by Smith *et al.* (2006) classifies joint behavior into four categories: brittle ($D \leq 2$), low ductility ($2 \leq D \leq 4$), medium ductility ($4 \leq D \leq 6$), and high ductility ($D > 6$).

The damping ratio indicates the amount of damping in the structure, which reduces and transmits input energy as the system undergoes deformation and progressive damage. The ability of a structure to absorb energy depends on its damping ratio. In this study, the damping ratio or equivalent viscous damping ratio (EVDR) was calculated according to ASTM E2126-02a using the following equation (ASTM, 2003a):

$$EVDR = \frac{HE}{2\pi PE} \quad (3)$$

where: $EVDR$ = equivalent viscous damping ratio; HE = hysteresis energy (Nmm); PE = potential energy (Nmm).

Modeling was performed using ABAQUS software (ABAQUS/Standard, 2009) to evaluate the capacity of the connection system tested under cyclic loads. Longitudinal elastic modulus E_L = 10.191 MPa was obtained from the test results. Simultaneously, E_R and E_T were calculated using the following relationship (TDMEC, 2005): E_R/E_L = 0.10, E_T/E_L = 0.05 with a friction coefficient value of 0.25–0.5 (Deta *et al.*, 2018). The friction coefficients vary across connection types: 0.25 and 0.5 for *Potanje*- and P-types, respectively, and 0.35 for both the modified D- and T-types (Table 3).

The modeling has several contact areas: beam–column, wedge–beam, wedge–column, wedge–wedge (modified D- and T-types), dowel–beam, and dowel–column. A

Table 3. Mechanical properties and friction coefficients

Mechanical properties	Connection type			
	Potanje-type	P-type	Modified D-type	Modified T-type
Density (kg/m^3)	1,040	1,040	1,040	1,040
Poisson's ratio (μ_{RT}, μ_{TL}, and μ_{RL})	0.24	0.24	0.24	0.24
Modulus of elastic E_L (MPa)	10,191	10,191	10,191	10,191
Modulus of elastic E_R (MPa)	1,019	1,019	1,019	1,019
Modulus of elastic E_T (MPa)	510	510	510	510
Shear modulus G_{LR} (MPa)	1,498	1,498	1,498	1,498
Shear modulus G_{LT} (MPa)	919	919	919	919
Shear modulus G_{RT} (MPa)	291	291	291	291
Friction coefficient at the contact surface (wood–wood)	0.25	0.50	0.35	0.35

mesh size of 20 was applied to the beam and column, whereas mesh sizes of four and five were applied to the dowels and wedges, respectively. Convergence was performed using the largest mesh 20. The generated error generated for the 20 mesh was 3.40% at a displacement of 100 mm. The Poisson's ratio values μ_{RT}, μ_{TL}, and μ_{RL} were adapted as 0.24 (Santoso *et al.*, 2021), while the maximum stress was 62 MPa. The G_{RT}, G_{TL}, and G_{RL} values were calculated using the following relationships (Hong, 2007):

$$G_{TL} = \frac{\sqrt{E_L \cdot E_T}}{2.\left(1+\sqrt{\mu_{LT}\mu_{TL}}\right.} \quad (4)$$

$$G_{RT} = \frac{\sqrt{E_R \cdot E_T}}{2.\left(1+\sqrt{\mu_{RT}\mu_{TR}}\right.} \quad (5)$$

$$G_{RL} = \frac{\sqrt{E_L \cdot E_R}}{2.\left(1+\sqrt{\mu_{LR}\mu_{RL}}\right.} \quad (6)$$

Plasticity (Zhang *et al.*, 2015) is a condition in which the strain does not fully return following stress release, leading to residual (plastic) strain. According to Song *et al.* (2010), a plastic limit is required for the constitutive relationship of wood parallel to the grains (Fig. 9) to fulfill specific requirements. These include: 1) identical tensile and compressive moduli, and 2) the absence of a significant plastic deformation stage prior to failure when the wood is subjected to tension parallel to the grain. The stress-strain curve is approximately linear, and the failure mode is brittle. When wood is subjected to compression parallel to the grain, a precise stage of plastic deformation occurs prior to failure due to the buckling instability of the wood grain.

3. RESULTS and DISCUSSION

3.1. Results

The moment–rotation curves for each connection type

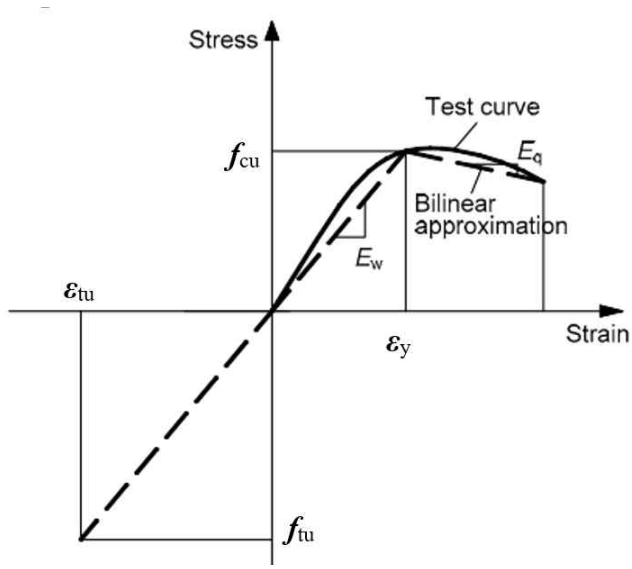

Fig. 9. Stress-strain curve for wood parallel to the grain. ε_y: yield strain of wood in compression; ε_{tu}: ultimate strain of timber in tension; f_{cu} and f_{tu}: ultimate stresses for compression and tension; E_w and E_q: elasticity and tangent moduli. Adapted from Zhang *et al.* (2015) with CC-BY-NC-ND.

obtained for the experiment (Fig. 10), provide valuable insights into the energy dissipation and deformation control during cyclic loading. The *Potanje*- and P-type connections exhibited higher moment capacities than the modified D- and T-type connections. With an increasing number of loading cycles, these two types showed

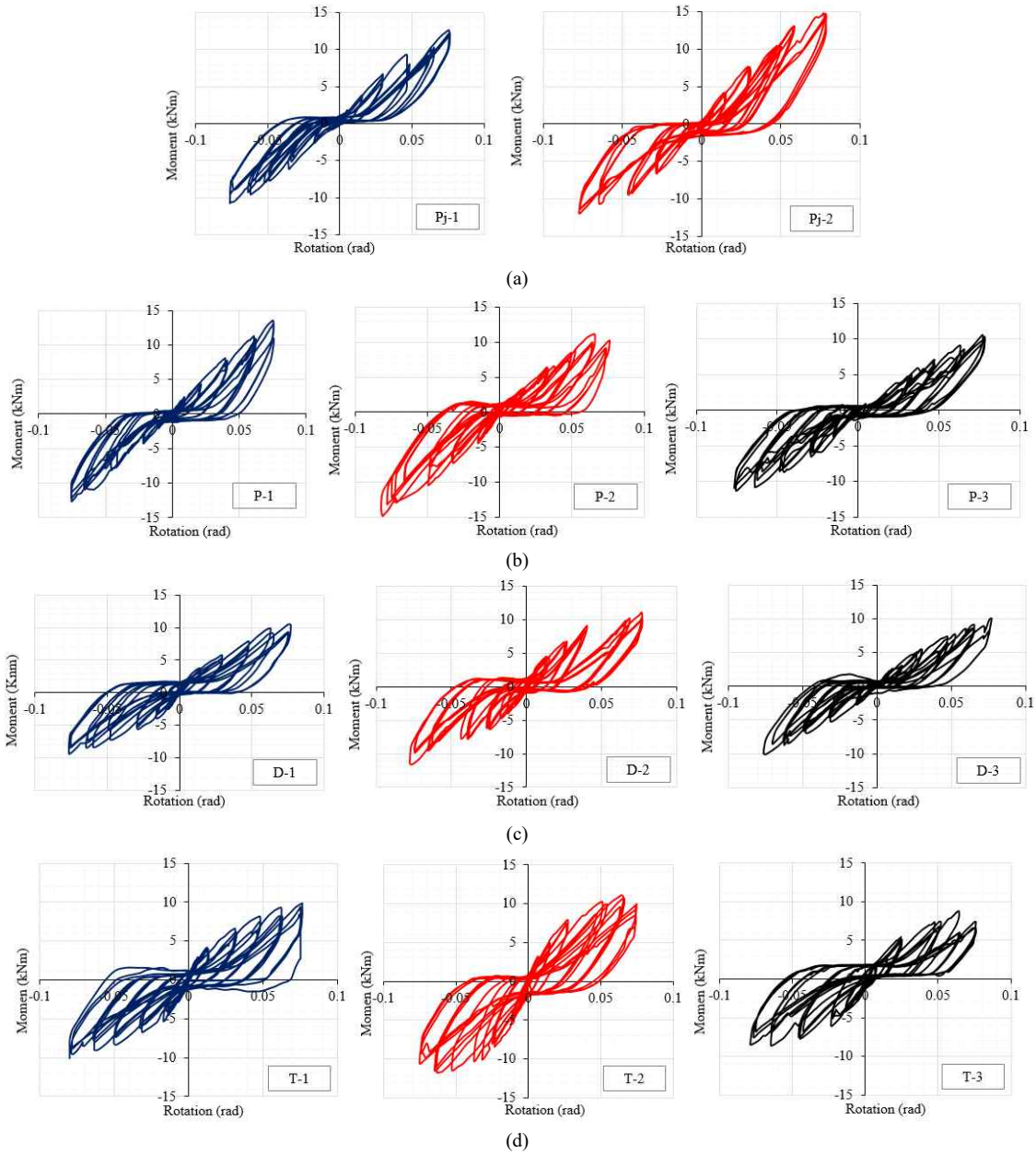

Fig. 10. Experimental test results showing the moment–rotation relationship. (a) *Potanje*-type, (b) P-type, (c) modified D-type, (d) modified T-type.

progressive flattening of the hysteresis loops, indicating reduced energy dissipation due to frictional degradation and sliding at the wedge interface. In comparison, the modified D- and T-type connections exhibited more gradual and stable hysteretic responses, with the T-type connections demonstrating superior damping resistance. As illustrated in Fig. 11, the EVDR of the modified T-type initially increased and remained approximately constant throughout the loading cycles, indicating sustained damping performance.

For all tested beam–column joint specimens, the achieved global rotation ranged between ± 0.075 and ± 0.079 rad at the last loading cycles (Table 4). At this rotation level, significant column displacements were observed at both the top and bottom of the column. The magnitude of the column displacement was relatively consistent across all joint configurations, indicating that the global deformation of the system was primarily governed by joint rotation. In comparison, the measured beam deformation was relatively small and varied among specimens. Beam displacement did not exhibit a clear linear relationship with the magnitude of the global rotation, suggesting that its contribution to the overall system deformation was limited compared to that of the column deformation.

The ductility values summarized in Table 5 show substantial differences among connection types. The modified T-type achieved the highest ductility among

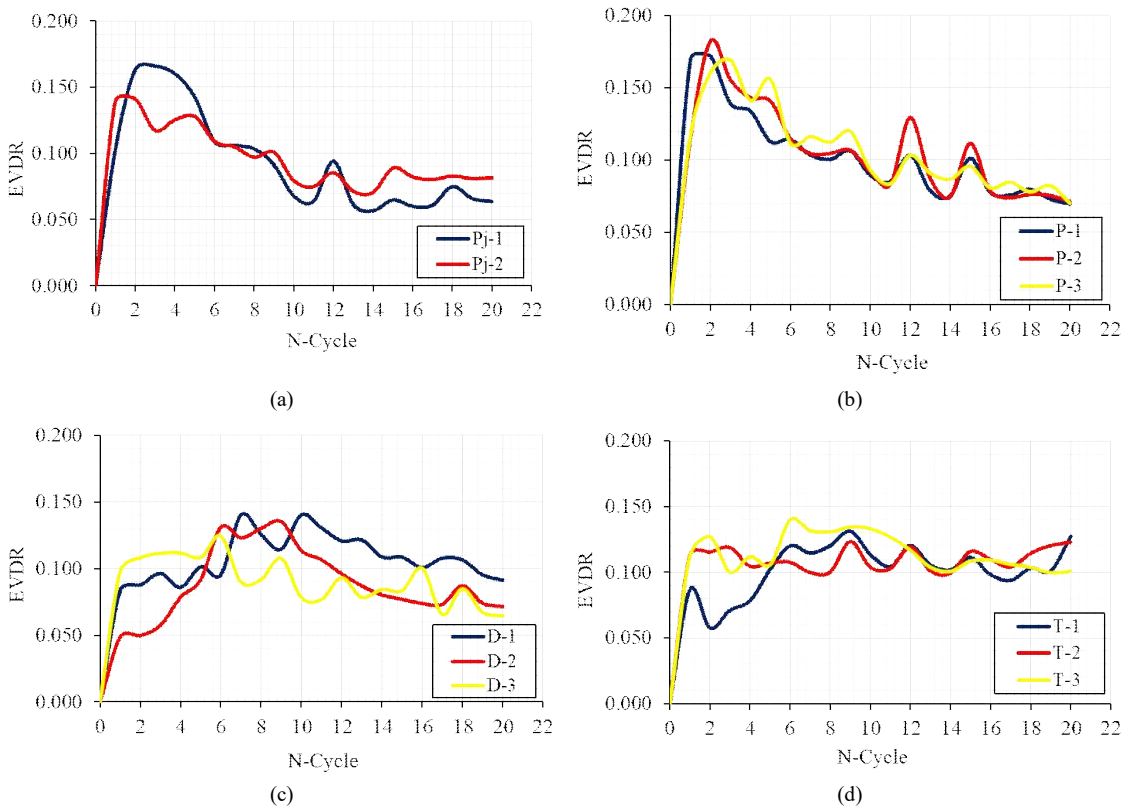

Fig. 11. Experimental test results showing the EVDR–N-cycle. (a) *Potanje*-type, (b) P-type, (c) modified D-type, (d) modified T-type. EVDR: equivalent viscous damping ratio.

Table 4. Column and beam displacements from experimental results

No.	Specimens	Rotation (rad)	Displacement at the column (mm)		Displacement at the beam (mm)
			Top	Bottom	
1	Pj-1	0.076	64.96	34.53	2.52
2	Pj-2	0.077	66.43	35.43	4.66
3	P-1	0.075	63.49	34.61	2.17
4	P-2	0.076	66.66	36.19	16.41
5	P-3	0.077	67.67	36.79	13.54
6	D-1	0.075	64.26	34.15	2.66
7	D-2	0.075	63.51	33.59	4.95
8	D-3	0.076	61.86	31.43	6.12
9	T-1	0.079	67.07	35.60	7.14
10	T-2	0.075	66.35	36.23	6.31
11	T-3	0.079	69.71	38.00	12.67

the tested configurations and was classified as medium ductility according to Smith *et al*. (2006). The modified D-type connections also exhibited improved ductility compared to that of the *Potanje*- and P-type connections. However, the P-type demonstrated the lowest ductility, indicating a limited capacity to sustain inelastic deformation and the occurrence of progressive degradation in energy absorption.

The finite element simulations, conducted in ABAQUS, showed strong correlation with the experimental observations. For both methods, the stress concentrations were primarily located in the wedge region, as illustrated in Fig. 12. The modified T-type exhibited the lowest maximum compressive stress at the wedge (22 MPa), while the *Potanje*-, P-, and modified D-types reached peak stresses of approximately 62 MPa.

The lateral load–displacement responses summarized in Table 6 further support these results. Although *Potanje*- and P-type connections reached higher peak lateral loads, they experienced faster degradation in the load-carrying capacity during repeated cycles. The modified D- and T-types produced lower peak loads but exhibited better displacement control and maintained their energy dissipation capacity.

The observed damage patterns at the column–wedge (Area A) and beam–column (Area B) interfaces (Fig. 13) were generally consistent between experimental testing and numerical simulation, confirming the validity of the modelling method. The differences between the experimental monotonic and numerical curves were recorded and attributed to the pinching effects observed during cyclic testing.

3.2. Discussion

The superior cyclic performance of the modified D- and T-type connections was primarily attributed to the interaction between the wedges and dowels. Specifically, the dowels effectively restricted beam sliding and reduced excessive slip at the wedge interface, thereby stabilizing the hysteresis behavior and preserving energy dissipation during repeated loading. In comparison, the

Table 5. Ductility value from the experimental results

No.	Specimens	Rotation (rad)		Ductility
		Yield	Ultimate	(D)
1	Pj-1	−0.032	−0.076	2.38
		0.028	0.076	2.71
2	Pj-2	−0.025	−0.077	3.07
		0.028	0.077	2.74
3	P-1	−0.035	−0.075	2.17
		0.033	0.075	2.30
4	P-2	−0.025	−0.075	2.96
		0.025	0.076	3.00
5	P-3	−0.027	−0.076	2.76
		0.034	0.077	2.24
6	D-1	−0.028	−0.076	2.73
		0.028	0.077	2.71
7	D-2	−0.022	−0.078	4.06
		0.019	0.077	3.51
8	D-3	−0.03	−0.076	2.55
		0.028	0.077	2.76
9	T-1	−0.016	−0.079	5.06
		0.020	0.076	3.80
10	T-2	−0.014	−0.063	4.52
		0.017	0.065	3.74
11	T-3	−0.014	−0.065	4.52
		0.020	0.064	3.18

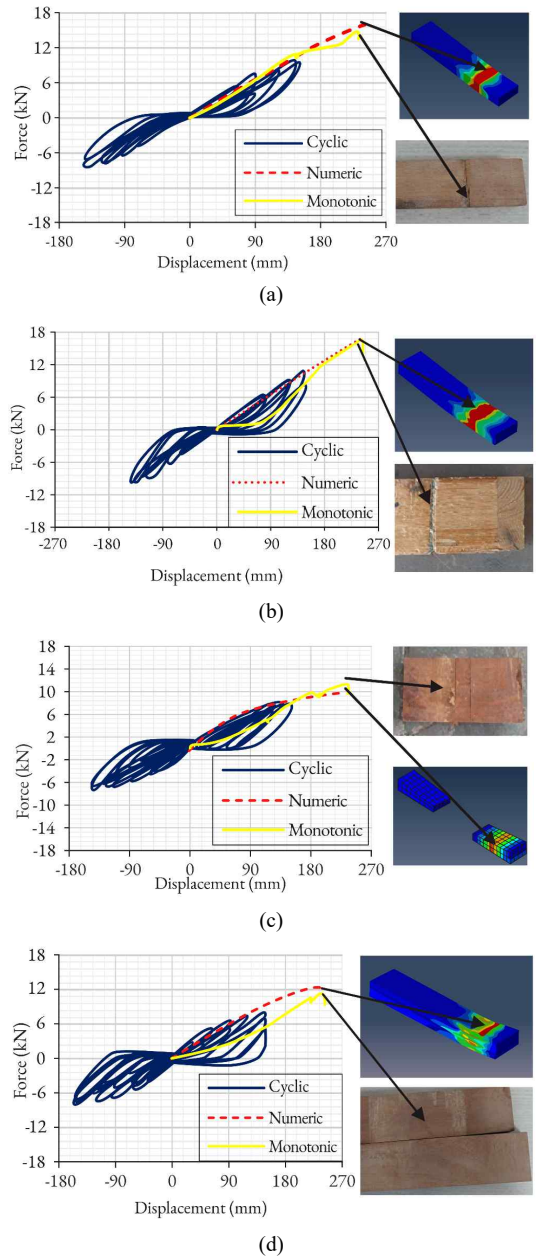

Fig. 12. Lateral force− displacement relationship. (a) *Potanje*-type, (b) P-type, (c) modified D-type, (d) modified T-type.

Potanje- and P-type connections depended predominantly on the frictional resistance at the wedge interface. As this interface deteriorated during cyclic loading, pinching became increasingly pronounced, resulting in a progressive loss of energy dissipation capacity and declining EVDR values. These results are consistent with those reported by Tanahashi *et al*. (2014) and Yeo *et al*. (2016).

Although the *Potanje*- and P-type connections achieved higher peak strengths, the modified D- and T-type connections provided significantly higher ductility and

Table 6. Relationship between experimental monotonic and numerical analysis

No.	Connection	Experimental monotonic		Numerical analysis		Lateral force difference (%)
		Lateral force (kNm)	Displacement (mm)	Lateral force (kNm)	Displacement (mm)	
1	*Potanje*-type	14.73	231.34	16.17	243.00	8.91
2	P-type	16.75	241.66	17.07	247.50	1.87
3	Modified D-type	11.22	236.93	12.30	231.66	8.78
4	Modified T-type	11.41	232.38	9.86	235.00	13.58

damping performance. Specifically, the modified T-type maintained stable EVDR values and exhibited the highest ductility, suggesting its superior suitability for seismically resistant timber structures. These results demonstrate that peak strength alone is insufficient for evaluating the seismic performance, suggesting the importance of the deformation capacity and stable hysteretic behavior as essential design parameters.

A previous study by Maeno *et al*. (2004) and Tanahashi *et al.* (2014) reported that traditional wedge connections function as friction-based dampers, owing to the bearing stresses induced during installation. The results demonstrated that the incorporation of dowels into wedge-based systems significantly improved deformation control and cyclic stability. The dominance of column displacement in the overall deformation response showed that the beam–column joint rotation was the primary mechanism controlling the global structural behavior. Within the tested rotation range, the observed deformations were mainly associated with shear mechanisms and progressive contact at the joint interface rather than with flexural deformation or rotation of the beam as an individual structural element.

The limited contribution of beam deformation to global rotation suggests that beam rotation plays a secondary role. Consequently, in a first-order analysis of the global response of beam–column joints, beam rotation can be considered negligible without significantly affecting the interpretation of the governing deformation mechanisms. These results provide a robust mechanical basis for simplifying the analytical models of traditional timber joints by emphasizing joint rotational behavior as a key parameter governing seismic response.

The improved performance of the modified D- and T-type connections suggests that these systems provide a practical and sustainable alternative for earthquake-resistant timber construction without relying on modern mechanical fasteners. The results demonstrate that traditional joinery systems can be adapted to satisfy modern seismic requirements, particularly in regions prone to strong ground motions. Moreover, the findings of the present study demonstrate the potential of timber as a sustainable structural material for seismic applications, supporting environmentally responsible building practices.

The differences between the experimental and numerical results are primarily related to the pinching phenomenon caused by nonlinear friction degradation and partial contact during cyclic loading, which cannot be fully represented as an ideal contact in the finite element model. Therefore, the numerical formulations require further refinement by incorporating nonlinear friction and contact conditions. Future studies should focus on shaking-table tests to validate these results under realistic earthquake loading conditions. Additionally, long-term studies examining the impact of environmental factors, such as moisture and temperature, on the performance of these connections will enable a more comprehensive understanding of their durability and reliability.

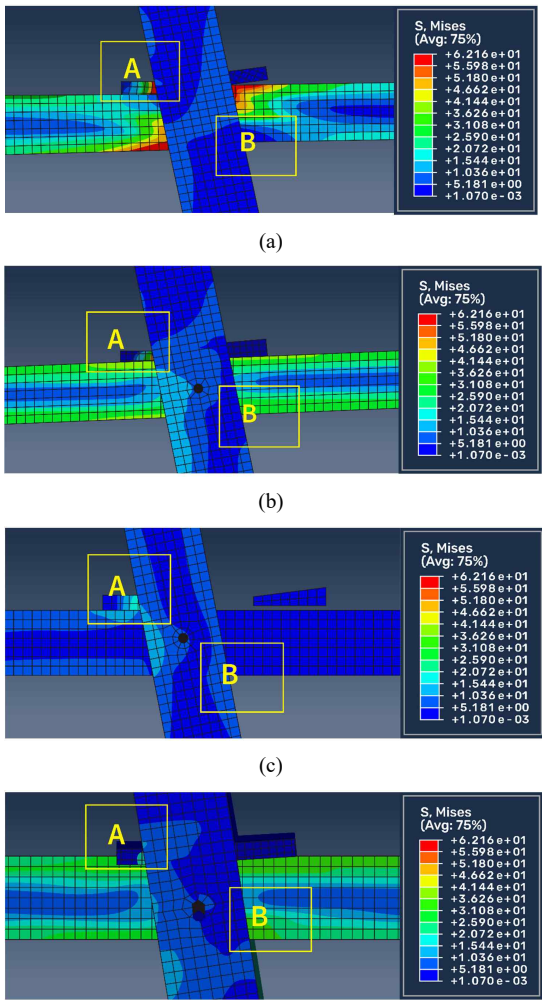

(a)

(b)

(c)

(d)

Fig. 13. Damage patterns due to columns–wedges surface contact (A), and beams–columns (B). (a) *Potanje*-type, (b) P-type, (c) modified D-type, (d) modified T-type.

4. CONCLUSIONS

In conclusion, this study demonstrates that the modified D- and T-type connections provide superior ductility and EVDR compared to those of the traditional *Potanje*- and P-type connections. The modified connections exhibited a superior performance under cyclic loading by maintaining stable damping resistance and energy absorption, which are essential for earthquake-resistant designs in timber structures. Although wedge remains the critical component responsible for energy dissipation and damage initiation, dowels enhance the performance by preventing excessive beam displacement. Among all connections, the modified T-type exhibited superior performance owing to its high ductility and consistent energy dissipation capabilities, making it suitable for seismic retrofitting and new construction in earthquake-prone regions. Although the *Potanje*- and P-type connections provide a higher peak strength, their effectiveness is reduced over multiple cycles owing to sliding and frictional degradation, which decreases their ability to dissipate energy. This study contributes to the development of sustainable earthquake-resistant solutions by demonstrating that reinforced traditional timber connections can provide superior seismic performance without relying on modern mechanical fasteners. The results support the integration of traditional materials and construction methods into modern seismic designs, contributing to a resilient infrastructure in seismic regions.

CONFLICT of INTEREST

No potential conflict of interest relevant to this article was reported.

ACKNOWLEDGMENT

This study was supported by a scholarship from the Indonesian Endowment Fund for Education Agency for a scholarship (LPDP).

REFERENCES

ABAQUS/Standard. 2009. User's Manual, Version 6.10. Hibbitt, Karlsson & Sorensen, Providence, RI, USA.

American Society for Testing and Materials [ASTM].

2003a. Standard Test Methods for Cyclic (Reserved) Load Test for Shear Resistance of Walls for Buildings. ASTM E2126-02a. ASTM International, West Conshohocken, PA, USA.

American Society for Testing and Materials [ASTM]. 1994. Standard Test Methods for Small Clear Specimens of Timber. ASTM D143-94. ASTM International, West Conshohocken, PA, USA.

American Society for Testing and Materials [ASTM]. 2003b. Standard Test Methods for Direct Moisture Content Measurement of Wood and Wood-base Materials (Reapproved 2003). ASTM D4442-92. ASTM International, West Conshohocken, PA, USA.

Cha, M.S., Yoon, S.J., Kwon, J.H., Byeon, H.S., Park, H.M. 2022. Mechanical properties of cork composite boards reinforced with metal, glass fiber, and carbon fiber. Journal of the Korean Wood Science and Technology 50(6): 427-435.

Deta, U.A., Suprapto, N., Mubarok, H., Adam, A.S., Kholiq, A. 2018. The comparison of static friction coefficient on wood between the combination of wood-metal load system and wood-sand load system. In: Bali, Indonesia, Proceedings of the International Conference on Science and Technology (ICST 2018), pp. 887-890.

Dong, H., Liang, X., Cao, W., Jin, Y. 2023. Seismic behavior of *mortise–tenon* joints reinforced with lightweight steel components. Journal of Building Engineering 65: 105755.

Fujita, K., Shin, E., Nishihama, J. 2016. Structural characteristics of traditional Japanese column and penetrating beam joint. In: Vienna, Austria, World Conference on Timber Engineering 2016.

Hadi, Y.S., Herliyana, E.N., Pari, G., Pari, R., Abdillah, I.B. 2022. Furfurylation effects on discoloration and physical-mechanical properties of wood from tropical plantation forests. Journal of the Korean Wood Science and Technology 50(1): 46-58.

Hassan, R., Ibrahim, A., Ahmad, Z. 2010. Performance of *mortise* and *tenon* connection fastened with wood and steel dowel. In: Trentino, Italy, World Conference on Timber Engineering.

Hong, J.P. 2007. Three-dimensional nonlinear finite element model for single and multiple dowel-type wood connections. Ph.D. Thesis, The University of British Columbia, Canada.

Kim, H.B., Yoshioka, T., Fujita, K., Ito, J., Nohara, H., Nohara, K., Narita, T., Lee, W., Hosokawa, A., Tanaka, T. 2024. Evaluation of bending creep performance of laminated veneer lumber (LVL) formwork for the design of timber concrete composite (TCC) structures. Journal of the Korean Wood Science and Technology 52(4): 375-382.

Lee, H.W., Jang, S.S. 2023. Lateral resistance of reinforced light-frame wood shear walls. Journal of the Korean Wood Science and Technology 51(1): 58-66.

Lee, M.D., Tang, R.W.C., Michael, Z., Khairulmaini, M., Roslan, A., Khodori, A.F., Sharudin, H., Lee, P.S. 2024. Physical and mechanical properties of light red meranti treated with boron preservatives. Journal of the Korean Wood Science and Technology 52(2): 157-174.

Li, H., Qiu, H., Wang, W. 2021. Experimental study on the mechanical performance of mortise-tenon joints reinforced with replaceable flat-steel jackets. Journal of Renewable Materials 9(6): 1111-1125.

Maeno, M., Suzuki, Y., Ohshita, T., Kitahara, A. 2004. Seismic response characteristics of traditional wooden frame by full-scale dynamic and static tests. In: Vancouver, BC, Canada, 13th World Conference on Earthquake Engineering.

Maras, M.M., Yurtseven, H.B., Ozdemir, M.F. 2024. Failure analysis of laminated wooden arches strengthened with novel carbon-fiber-reinforced polymer (CFRP) composites: an experimental study. Journal of the Korean Wood Science and Technology 52(6): 585-604.

Mawardi, I., Nurdin, N., Razak, H., Amalia, I., Sariyusda, S., Aljufri, A., Jaya, R.P. 2025. Development of lightweight engineered wood produced from derived sugarcane bagasse and coir fiber: Evaluation of the bending and thermal properties. Journal of the Korean Wood Science and Technology 53(1): 1-13.

Muñoz, W., Mohammad, M., Salenikovich, A., Quenneville, P. 2008. Determination of yield point and ductility of timber assemblies: In search for a harmonised approach. Ph.D. Thesis, University of Lisbon, Portugal.

Nugroho, W.D., Na'iem, M., Lukmandaru, G., Widiyatno, Feriawan, Y., Prastiwi, F.W., Wibowo, A., Puspitasari, D. 2024. Physical and mechanical properties of 20-year-old clonal teak trees in Ngawi, East Java, Indonesia. Journal of the Korean Wood Science and Technology 52(5): 459-472.

Pusat Studi Gempa Nasional [PuSGeN]. 2018. Kajian Gempa Palu Sulawesi Tengah (in Bahasa). Ministry of Public Works and Housing of the Republic of Indonesia, Bandung, Indonesia.

Rofii, M.N., Mairing, M.J., Listyanto, T., Sumardi, I., Hartono, R. 2024. Physical and mechanical properties of laminated board from Betung bamboo (*Dendrocalamus asper*). Journal of the Korean Wood Science and Technology 52(4): 383-392.

Santoso, M.Y., Putri, K.I., Sandora, R. 2021. Penentuan faktor keamanan material ganjal kapal untuk dok galangan kapal. Jurnal Poli-Teknologi 20(2): 153-159.

Seta, G.M., Hidayati, F., Widiyatno, Na'iem, M. 2023. Wood physical and mechanical properties of clonal teak (*Tectona grandis*) stands under different thinning and pruning intensity levels planted in Java, Indonesia. Journal of the Korean Wood Science and Technology 51(2): 109-132.

Smith, I., Asiz, A., Snow, M., Chui, Y.H. 2006. Possible Canadian/ISO approach to deriving design values from test data. In: Florence, Italy, Proceedings of the 39th CIB Working Commission W18: Timber Structures.

Song, D.B., Kim, K.H. 2023. Influence of composition of layer layout on bending and compression strength performance of larix cross-laminated timber (CLT). Journal of the Korean Wood Science and Technology 51(4): 239-252.

Song, X., Lam, F., Huang, H. 2010. Stability capacity of metal plate connected wood truss assemblies. Journal of Structural Engineering 136(6): 723-730.

Suesada, H., Miyamoto, K., Shibusawa, T., Aoki, K., Inayama, M. 2019. Reinforcing effect of hardwoods on the moment resistance performance of traditional Japanese "nuki"-column joints. Journal of Wood Science 65(1): 65.

Tanahashi, H., Ooka, Y., Izuno, K., Suzuki, Y. 2014. Seismic resisting mechanism and formulations of traditional wooden joints with wedges. In: Quebec City, QC, Canada, World Conference on Timber Engineering.

Timberwork Design Manual Editing Committee [TDMEC]. 2005. Timberwork Design Manual. 3rd ed. China Architecture & Building Press, Beijing, China.

Wu, G., Gong, M., Gong, Y., Ren, H., Zhong, Y. 2019. Mechanical performance of mortise and tenon joints pre-reinforced with slot-in bamboo scrimber plates. Journal of Wood Science 65: 38.

Yeo, S.Y., Kitamori, A., Aoyama, T., Chung, Y.L., Mori, T., Hsu, M.F., Komatsu, K., Isoda, H. 2016. Lateral shear performance of traditional Taiwanese timber column with half and full-penentrating beam. In: Vienna, Austria, World Conference on Timber Engineering.

Yu, S., Pan, W., Su, H., Ye, L., Wang, D. 2022. Experimental study on tenon and mortise joints of wood-structure houses reinforced by innovative metal dampers. Forests 13(8): 1177.

Zhang, J., Xu, Q., Xu, Y., Zhang, M. 2015. Research on residual bending capacities of used wood members based on the correlation between non-destructive testing results and the mechanical properties of wood. Journal of Zhejiang University-Science A 16(7): 541-550.